第 32 卷第 10 期 无 机 化 学 学 报 Vol.32 No.10
2016 年 10 月 CHINESE JOURNAL OF INORGANIC CHEMISTRY 1816-1824

$Ru/Ce(OH)CO_3$ 纳米复合材料催化氨硼烷水解产氢

陈健民 卢章辉* 熊丽华
(江西师范大学化学化工学院无机膜材料工程技术研究中心,南昌 330022)

摘要: 采用一种简单的方法快速合成了 $Ru/Ce(OH)CO_3$ 纳米复合材料。基于 TG,XRD,TEM,EDX,XPS 和 ICP 等方法详细表征了所制备的催化剂,并用于催化氨硼烷水解制氢。表征结果表明尺寸大约为 4.8 nm 的 Ru 纳米粒子高度分散在 $Ce(OH)CO_3$ 纳米棒上。该催化剂对于氨硼烷水解制氢表现出优异的催化性能,在室温下其转化频率(TOF)达到 389.6 $mol_{H_2}\cdot mol_{Ru}^{-1}\cdot min^{-1}$。而且该催化剂循环使用 11 次之后依然能够对氨硼烷催化产氢保持很高的活性。

关键词: 能源材料; 氨硼烷; 稀土; 催化水解; 制氢
中图分类号: O643.36 **文献标识码**: A **文章编号**: 1001-4861(2016)10-1816-09
DOI:10.11862/CJIC.2016.228

Hydrolysis of Ammonia Borane by $Ru/Ce(OH)CO_3$ Nanocomposites for Hydrogen Production

CHEN Jian-Min LU Zhang-Hui* XIONG Li-Hua
(*Jiangxi Inorganic Membrane Materials Engineering Research Centre, College of Chemistry and Chemical Engineering, Jiangxi Normal University, Nanchang* 330022, *China*)

Abstract: A facile method for fabrication of $Ru/Ce(OH)CO_3$ nanocomposites (NCs) under mild conditions was reported. The as-synthesized catalysts were characterized by TG, XRD, TEM, EDX, XPS, ICP, and used for H_2 production from hydrolysis of ammonia borane (AB). All the characterized results exhibit that Ru nanoparticles (NPs) around 4.8 nm are highly dispersed on $Ce(OH)CO_3$ nanorods. The as-synthesized $Ru/Ce(OH)CO_3$ NCs show a high catalytic activity for hydrogen generation from the aqueous of ammonia borane complex with a turnover frequency (TOF) of 389.6 $mol_{H_2}\cdot mol_{Ru}^{-1}\cdot min^{-1}$ at room temperature, being higher than that of most reported metal-based catalysts. Especially, the catalyst can keep a superior activity for hydrolysis of AB even after eleven times of recycle.

Keywords: energy storage materials; ammonia borane; rare earth oxide; catalytic hydrolysis; hydrogen generation

0 Introduction

Ammonia borane (NH_3BH_3, AB) complex has been identified as one of the most attractive candidates for on-board portable hydrogen applications among all other practical hydrogen storage materials due to its high hydrogen content (19.6%, *w*/*w*), low molecular weight, high stability under ambient condition, and environmentally friendly nature[1-7]. More importantly, hydrogen stored in AB can be released at an appreciable rate via hydrolysis in the presence of a suitable catalyst, which appears to be the most

收稿日期:2016-03-30。收修改稿日期:2016-09-05。
国家自然科学基金(No.21463012)和江西省自然科学基金(No.2016BAB203087)资助项目。
*通信联系人。E-mail:luzh@jxnu.edu.cn;会员登记号:S06N7731M1111。

convenient one for portable hydrogen storage application[8-10]. The catalytic hydrolysis reaction can be briefly expressed as follows:

$$NH_3BH_3+2H_2O \rightarrow NH_4^++BO_2^-+3H_2$$

To date, a number of catalyst systems have been tested in the hydrolysis of AB, such as noble metals Au[11], Pt[12-14], Ru[15-17], Rh[18-20], Pd[21,22], Ag[23], and non-noble metals Cu[24-27], Fe[28-31], Ni[32-34], Co[35-38]. Although metal in nano-size show a higher catalytic activity, they easily aggregate into clumps during the catalytic processes due to their high surface energy, resulting in a large reduction of their catalytic activity or inactivation[12]. For the development of heterogeneous catalysts, decreasing the size of the catalyst and preventing aggregation are the keys to obtaining high catalytic activity. One strategy to achieve this goal is to immobilize the catalyst onto specific supports[18]. In recent years, rare earth compounds have been widely applied in catalysis, fuel cells, optical materials, gas sensors, and chemical materials due to their specific property. In particularly, cerium oxides have been successfully used as carriers to support noble metal nanoparticles (NPs)[39]. To our knowledge, there are few reports about using the cerium hydroxide carbonate (Ce(OH)CO_3) as the support for immobilize the metal NPs.

In this work, we report a facile synthesis of Ru/Ce(OH)CO_3 nanocomposites (NCs) under mild condition. Neither additional functional molecules nor stabilizing molecules are employed during the whole preparation. The as-synthesized catalysts exert a higher catalytic activity than most of reported metal NPs in the hydrolytic dehydrogenation of AB. The high catalytic activity and good durability of the Ru/Ce(OH)CO_3 NCs make them a very promising candidate to be used as catalyst in the practical application hydrogen generation systems using AB as solid hydrogen storage material.

1 Experimental

1.1 Materials

Ammonia borane (NH_3BH_3, Aldrich, 90%), hexaammine ruthenium(Ⅲ) chloride (Ru $(NH_3)_6Cl_3$, J&K Scientific Ltd., 97.5%), cerium(Ⅲ) nitrate hexahydrate, ($Ce(NO_3)_3\cdot 6H_2O$, J&K Scientific Ltd., 99.5%), urea ($CO(NH_2)_2$, Aladdin, 99%), sodium borohydride ($NaBH_4$, Aldrich, 99.9%) were all used without further purification. Ultrapure water with the specific resistance of 18.3 MΩ·cm was obtained by reversed osmosis followed by ion exchange and filtration.

1.2 Synthesis of Ru/Ce(OH)CO_3 NCs

Ce(OH)CO_3 nanorods was prepared by a slight modification of a recipe described previously[40-42]. In a typical synthesis, calculated amounts of aqueous solutions of Ru$(NH_3)_6Cl_3$ (6 mL, 3.26 mg) corresponding to 6.0 % (*w*/*w*, the same below) Ru loading were added to 16.8 mg of as-prepared Ce(OH)CO_3 nanorods under stirring. The mixture was kept at 90 ℃ for 3 h, followed by washing with water and then reduced by freshly aqueous solution of $NaBH_4$ (3 mg, 5 mL). After a few minute, a grey suspension of Ru/Ce(OH)CO_3 NCs were obtained and then used as the catalyst for the catalytic reaction. The other four samples with different Ru loadings (2%, 4%, 8% and 10%) were also prepared using the above method by changing the amount of Ce(OH)CO_3.

For comparison, Ru NPs with different supports (such as C, Al_2O_3, SiO_2, CeO_2, and Ce(OH)CO_3) were also prepared by the impregnation method (IMP). 2.6 mg of $RuCl_3$ and 16.8 mg of different supports were add into the 5 mL of water solution, and then the solution was stirred and sonicated at room temperature for 30 min. Afterward, 3 mg of $NaBH_4$ was added into the above obtained solution with vigorous stirring. After 5 min, the black product were obtained, and then used as catalyst for the catalytic reaction. The Ru loading is 6.0 % in order to obtain similar active particles.

1.3 Material characterization

The powder X-ray diffraction (XRD) was performed on a Rigaku RINT-2200 X-ray diffractometer with a Cu $K\alpha$ (λ=0.154 05 nm) source (40 kV, 20 mA) to determine the structure of these catalysts. Scanning electron microscope (SEM, Hitachi, SU8020) image was taken on a cold field-emission instrument to survey the morphology of catalyst (5 kV). Transmission

electron microscope (TEM), energy-dispersive X-ray spectroscopy (EDX), were observed using transmission electron microscope (TEM, JEM-2100) operating at 200 kV. The TEM samples were dispersed in ethanol by sonication 30 min, and then one droplet of the nanoparticle suspension was dropped onto a carbon-coated copper grid and dried in air. X-ray photoelectron spectroscopy (XPS) was carried out on an ESCALABMKLL X-ray photoelectron spectrometer with Al $K\alpha$ radiation. The weight content of Ru in Ru/$Ce(OH)CO_3$ NCs was analyzed by means of a 725-ES inductively coupled plasma (ICP) spectrophotometer (Varian Corp). Thermogravimetric analyses (TG) was carried out with a Netzsch-409 STA simultaneous TG-DTA apparatus with a heating rate of 10 ℃·min^{-1} under flowing air.

1.4 Catalytic activity

Catalytic reactions were carried out at room temperature using a two-necked round bottom flask with one of the flask openings connected to a gas burette and the other for the introduction of AB. During the reaction, the flask was placed in a thermostat that was equipped with a water circulating system to maintain the reaction temperature (25 ℃), usually within ±0.5 ℃. Then 1 mmol AB (34.30 mg) was added into the reaction vessel and the reactant was quickly stirred with a magnetic stirrer during the reaction. The volume of hydrogen gas was evaluated in a typical water-filled graduated burette system.

1.5 Kinetic studies of hydrolytic dehydrogenation of AB catalyzed by Ru/$Ce(OH)CO_3$ NCs

Sets of experiments were carried out to establish the rate law for catalytic hydrolysis of AB in aqueous solution using Ru/$Ce(OH)CO_3$ NCs as catalyst. In the first set of experiments, different concentrations of Ru (0.35, 0.69, 1.04, and 1.38 mmol·L^{-1}) were performed at room temperature while the AB concentration was kept the same (200 mmol·L^{-1}). In the second set of experiments, different concentrations of AB (100, 200, 300, and 400 mmol·L^{-1}) were performed at room temperature while the Ru concentration was kept the same (1.38 mmol·L^{-1}). Finally, the reaction temperature was varied at 20, 25, 30, and 35 ℃ while the molar ratio of n_{Ru}/n_{AB} was kept constant of 0.006 9.

1.6 Durability test

For durability test, catalytic reactions were repeated 11 times at room temperature by adding another equivalent of AB (1 mmol) into the reactor after the previous cycle. The molar ratio of Ru to AB was kept at 0.006 9 during each cycle test.

2 Result and discussion

2.1 Catalyst characterization

According to the TG/DTA analysis, the $Ce(OH)CO_3$ material is stable under the temperature less than 280 ℃ (Fig.S1). Therefore, the synthesized $Ce(OH)CO_3$ can be used as the support for nanocatalysts. The as-synthesized Ru/$Ce(OH)CO_3$ NCs were characterized by ICP, TG, XRD, TEM, HRTEM, EDX, and XPS. The contents of Ru in the Ru/$Ce(OH)CO_3$ NCs were determined to be 6.0 % by ICP measurements (Table S1). The XRD patterns of the as-synthesized $Ce(OH)CO_3$, Ru NPs, Ru/$Ce(OH)CO_3$ NCs before and after calcination are presented in Fig.1, respectively. As shown in Fig.1a, all peaks in this pattern can be well-indexed to a pure phase of $Ce(OH)CO_3$, which is in good agreement with the PDF file for $Ce(OH)CO_3$ (PDF No. 41-0013). Similar diffraction peaks are also observed in Ru/$Ce(OH)CO_3$ NCs, indicating that host materials almost remain intact after the loading of Ru NPs. For free Ru NPs (Fig.1c), the diffraction peak 2θ=44.0°

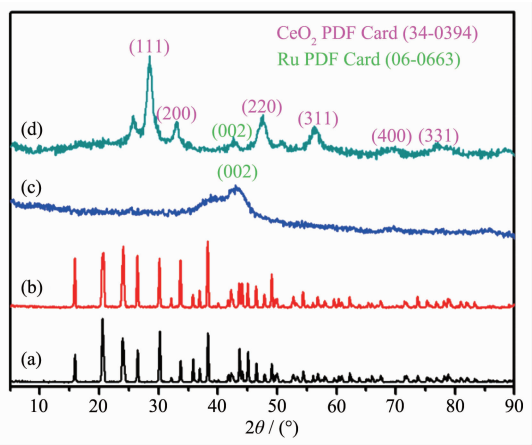

Fig.1 XRD patterns of the samples: (a) $Ce(OH)CO_3$ nanorods; (b) Ru/$Ce(OH)CO_3$ NCs; (c) Ru NPs; (d) Ru/$Ce(OH)CO_3$ NCs after heat treatment at 450 ℃ for 2 h in argon atmosphere

attributed to Ru was observed. No distinct diffraction peaks attributed to Ru were detected from the XRD pattern of $Ru/Ce(OH)CO_3$ NCs (Fig.1b), which might be due to the fact that the loading of Ru is too small and the diffraction peaks of Ru NPs are covered by $Ce(OH)CO_3$. To get the XRD information of Ru specie in the NCs, we have tested $Ru/Ce(OH)CO_3$ NCs with a high metal loading of 60.0%[43-44] (Fig.S2c). It is found that obvious diffraction peak of Ru show up, indicating the existence of Ru in the NCs. As for $Ru/Ce(OH)CO_3$ NCs with a Ru loading of 6.0%, after heated treatment at 450 ℃ for 2 h in argon atmosphere, Ru and CeO_2 with pure face-centered cubic (*fcc*) structure are observed (Fig.1d).

The microstructure of $Ru/Ce(OH)CO_3$ NCs were fully analyzed by SEM, TEM, HRTEM, and EDX observations. The TEM and SEM images of $Ce(OH)CO_3$ are shown in Fig.S3 and S4, respectively. The rod-like $Ce(OH)CO_3$ support with 150~350 nm in diameter, tens of nanometers in length, and smooth surface are observed. As shown in Fig.S5, the SEM images of the as-prepared $Ru/Ce(OH)CO_3$ NCs display the rougher surface of $Ce(OH)CO_3$, indicating that Ru NPs are immobilized on the surface of $Ce(OH)CO_3$. When the Ru loading increases from 2% to 10%, the size of the metal NPs supported on $Ce(OH)CO_3$ grows gradually. Especially, the SEM images of $Ru/Ce(OH)CO_3$ NCs with a high Ru loading 8% and 10% show a large particle aggregation on the surface of $Ce(OH)CO_3$. The TEM images of 6% $Ru/Ce(OH)CO_3$ NCs are shown in Fig.2a~c. It can be found that the round and dark points of Ru NPs are embedded and highly dispersed

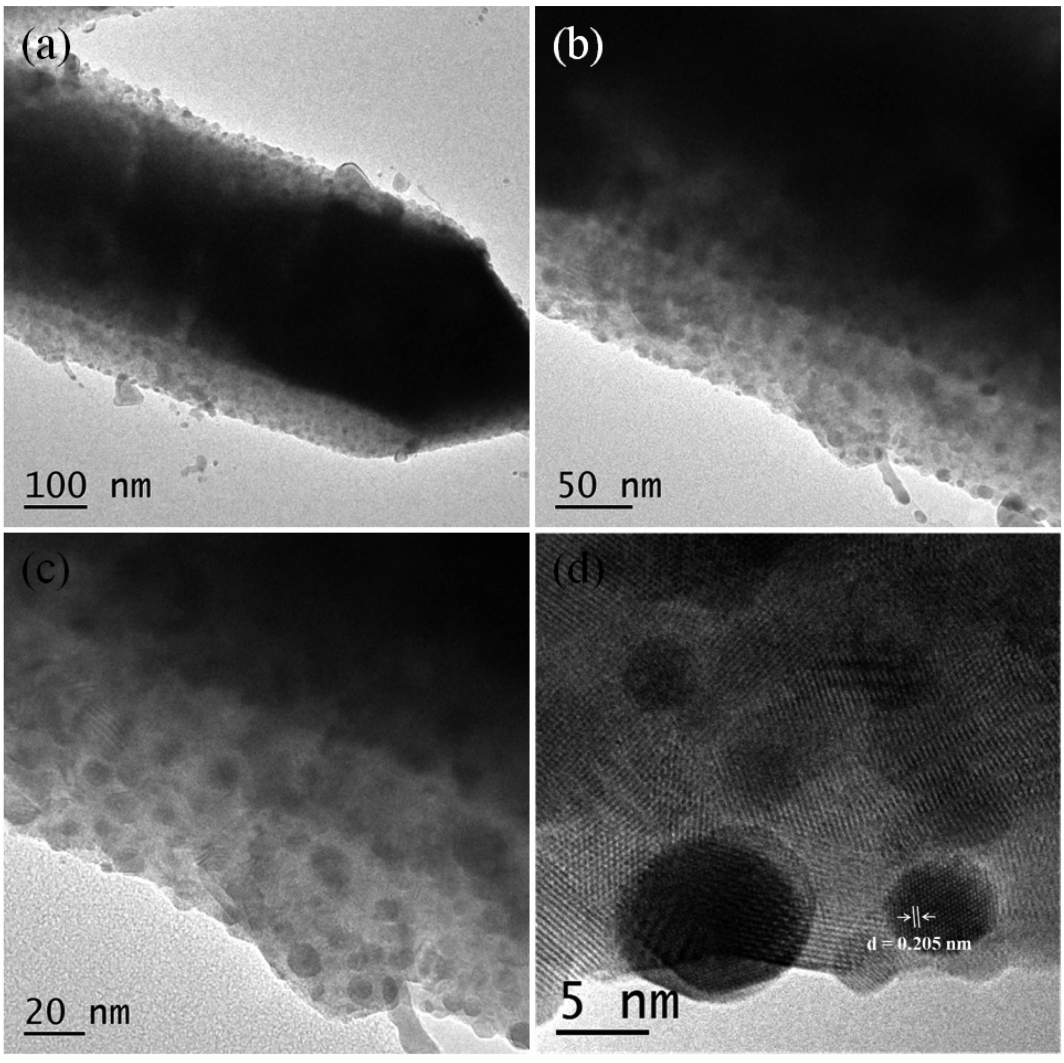

Fig.2　TEM (a~c) and HR-TEM (d) images of $Ru/Ce(OH)CO_3$ NCs

on the gray rods of $Ce(OH)CO_3$, which can help to prevent the agglomeration of Ru NPs. The lattice fringes can be observed in the high-resolution TEM (HRTEM) image (Fig.2d). Fig.2d shows the *d* spacing of 0.205 nm, which is consistent with the (101) plane of Ru. Furthermore, the HRTEM image shows that the as-prepared Ru NPs with the size of about 4.8 nm. The TEM-EDX spectrum was shown in Fig.S6, indicating that ruthenium is the only element detected in the sample in addition to the framework elements of $Ce(OH)CO_3$ (Ce, C, O). Ru/$Ce(OH)CO_3$-IMP can be prepared by impregnation method with the $Ce(OH)CO_3$ and $RuCl_3$. The representative SEM image of Ru/Ce $(OH)CO_3$-IMP is shown in Fig.S7. A similar morphology was observed as for Ru/$Ce(OH)CO_3$ NCs (Fig.S5). The compositions of Ru and Ce in the Ru/$Ce(OH)CO_3$-IMP is 0.006 9 and 0.073 6 mmol, which are quite close to the initial amount of Ru and Ce, respectively.

Additionally, XPS is applied to confirm the presence of metallic ruthenium, which reveal that the Ru is the only element detected in addition to the $Ce(OH)CO_3$ framework elements (C, O, Ce) (Fig.3a). The results are well agreed with the EDX results. As shown in Fig.3b, the XPS spectrum consists of C1*s* peaks and Ru3*d* doublets. The peak-fitting of Ru3*d* core level reveals four peaks, the peaks at 279.9 ($Ru3d_{5/2}$) and 283.6 eV ($Ru3d_{3/2}$) are attributed to Ru^0 [45-46]. While the other two peaks at 280.7 and 285.7 eV stand for oxidized Ru[47-48], which may originate from the oxidation of the Ru NPs upon exposure to air. The former peak at 284.4 eV, covered by the signal of C1*s*, is consistent with binding energy values related to $Ru3d_{3/2}$[46]. Additionally, C1*s* peak at 288.4 eV (C=O) is observed in the XPS. In summary, the nanocatalysts appeared to consist of Ru^0 and RuO_2 embedded on $Ce(OH)CO_3$. It should be noted that the partial oxidation of Ru should not exert significant influence on the catalytic activity of the Ru/$Ce(OH)CO_3$ NCs catalyst because of the inactive RuO_2 might be reduced back to Ru^0 by AB or $NaBH_4$[49]. Furthermore, XPS analysis is applied

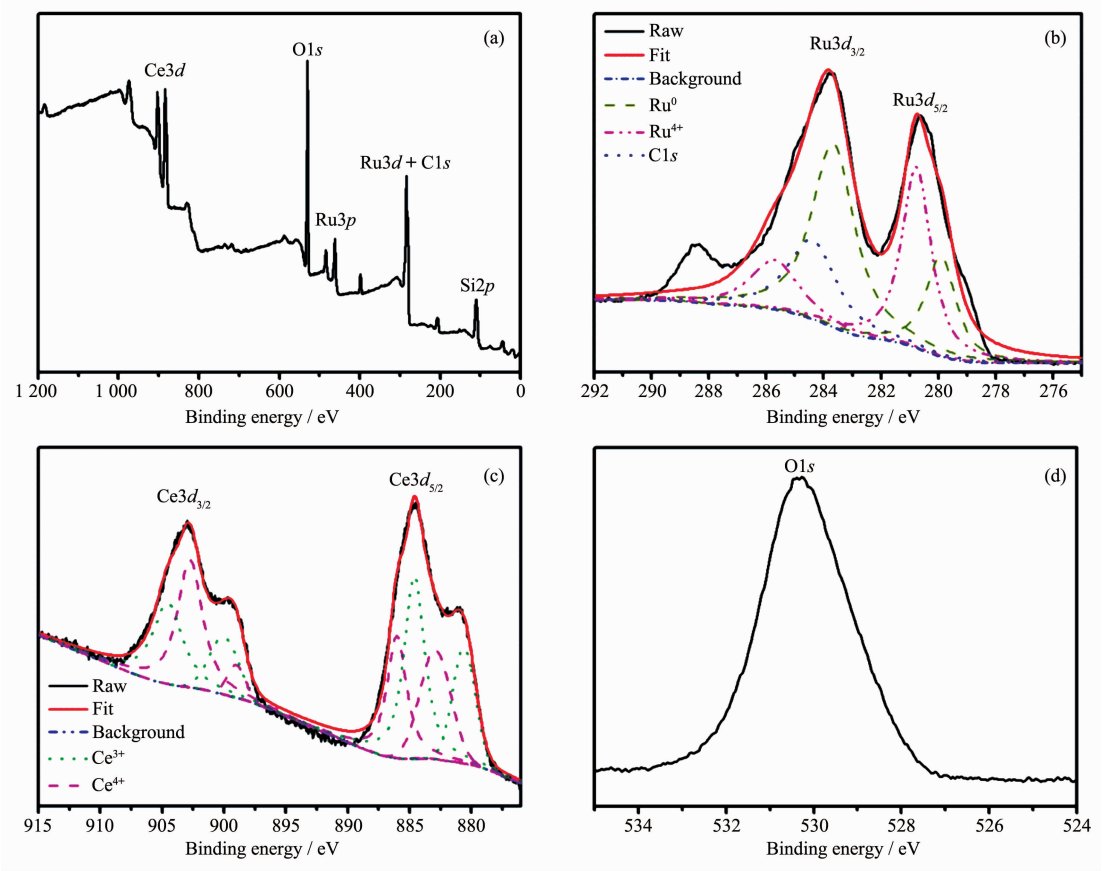

Fig.3 Survey XPS spectrum of Ru/$Ce(OH)CO_3$ NCs(a) and the high resolution XPS spectra of Ru3*d*, Ce3*d*, and O1*s* of Ru/$Ce(OH)CO_3$ NCs(b~d)

for the sample with Ce (Fig.3c) and O (Fig.3d). It can be seen that, in this sample, Ce has the oxidized states of Ce^{3+} and Ce^{4+}. The peak of O1*s* located at about 530.5 eV is due to the chemisorbed oxygen caused by $Ce(OH)CO_3$. It is reported that the oxygen defect structure of cerium oxide is dynamic and may change spontaneously due to physical parameters such as temperature, presence of other ions, and partial pressure of oxygen[50-51]. Therefore, the existences of Ce^{3+} and Ce^{4+} in the sample are reasonable.

2.2 Catalytic activities for hydrolysis of AB

Catalytic activity of the prepared $Ru/Ce(OH)CO_3$ NCs together with $Ru/Ce(OH)CO_3$-IMP, Ru/C-IMP, Ru/Al_2O_3-IMP, Ru/SiO_2-IMP, and Ru/CeO_2-IMP have been investigated for the hydrolysis of AB aqueous solution at 25 ℃ (n_{Ru} / n_{AB}=0.006 9). As shown in Fig.4, the H_2 generation rate from aqueous AB significantly depends on different catalysts. No hydrogen generation was observed for $Ce(OH)CO_3$, indicating that $Ce(OH)CO_3$ is inactive for hydrolysis of AB. The Ru/C-IMP, Ru/Al_2O_3-IMP, Ru/SiO_2-IMP, Ru/CeO_2-IMP and $Ru/Ce(OH)CO_3$-IMP catalysts show a lower catalytic activity, as compared to the activity of $Ru/Ce(OH)CO_3$ NCs. Evidently, the as-synthesized $Ru/Ce(OH)CO_3$ NCs show an excellent catalytic activity (1.1 min) with a total TOF value as high as 389.6 $mol_{H_2}\cdot mol_{Ru}^{-1}\cdot min^{-1}$, relatively high values for hydrolytic dehydrogenation of AB (Table S2)[12,15,17-19,21,25-26,52-60]. The highly catalytic activity of $Ru/Ce(OH)CO_3$ NCs are attributed to high dispersion of Ru NPs on the $Ce(OH)CO_3$ nanorod. The formation of highly disperse Ru supported on $Ce(OH)CO_3$ nanorod may be due to a reaction between $Ru(NH_3)_6Cl_3$ and $Ce(OH)CO_3$ at 90 ℃[42]. In addition, $Ru/Ce(OH)CO_3$-IMP and Ru/CeO_2-IMP prepared with $Ru(NH_3)_6Cl_3$ precursor show a lower catalytic activity than those of $Ru/Ce(OH)CO_3$-IMP and Ru/CeO_2-IMP prepared with $RuCl_3$ precursor (Fig.S8). The $Ru/Ce(OH)CO_3$ NCs with a Ru loading of 6.0% (Fig.S9) displays a superior catalytic performance for the generation of hydrogen amongst all the $Ru/Ce(OH)CO_3$ catalysts with different Ru weight. Furthermore, the as-synthesized $Ru/Ce(OH)CO_3$ NCs show a robust durability for hydrolysis of AB even after eleven times of recycle (Fig.S10). The observed activity loss is probably due to the fact that the increase viscosity of the solution and/or deactivation effect of the increasing metaborate concentration during the hydrolysis of AB[7].

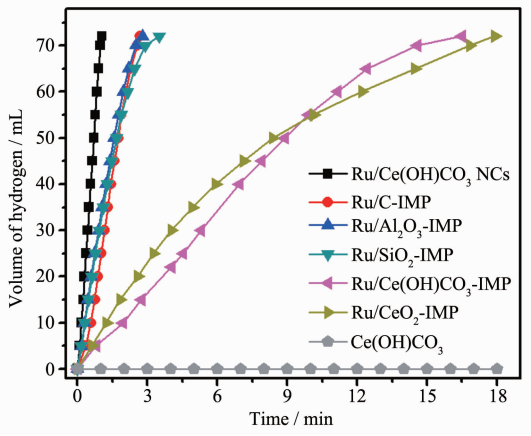

Fig.4 Plots of the volume of hydrogen generation from AB hydrolysis as a function of time catalyzed by $Ru/Ce(OH)CO_3$ NCs, Ru/C-IMP, Ru/Al_2O_3-IMP, Ru/SiO_2-IMP, $Ru/Ce(OH)CO_3$-IMP, Ru/CeO_2-IMP, and $Ce(OH)CO_3$ at 25 ℃, respectively (n_{Ru}/n_{AB}= 0.006 9)

As shown in the Fig.S11, the $Ru/Ce(OH)CO_3$ NCs after heat treatment at 450 ℃ for 2 h in argon atmosphere (*i.e.* Ru/CeO_2) have been investigated for the hydrogen generation from AB (200 $mmol\cdot L^{-1}$, 5 mL). A stoichiometric amount of hydrogen (72 mL) is evolved in 10.2 min. Obviously, $Ru/Ce(OH)CO_3$ NCs after heated in the Ar atmosphere (*i.e.* Ru/CeO_2) exhibit a lower catalytic performance, in comparison to $Ru/Ce(OH)CO_3$ NCs, for the dehydrogenation of AB. The low activity of $Ru/Ce(OH)CO_3$ NCs after calcination could be attributed to the thermal decomposition of $Ce(OH)CO_3$ and the aggregated of Ru.

Three set of experiments about catalyst concentration, AB concentration, and temperature were carried out to investigate the kinetics of $Ru/Ce(OH)CO_3$ NCs toward hydrolysis of AB. Fig.5a shows the plot of the evolution of equivalent hydrogen per mole of AB versus time for the hydrolysis of AB using $Ru/Ce(OH)CO_3$ NCs as the catalyst in different Ru concentrations. When the catalyst concentration increases, the reaction time decreases obviously from 4.35 min

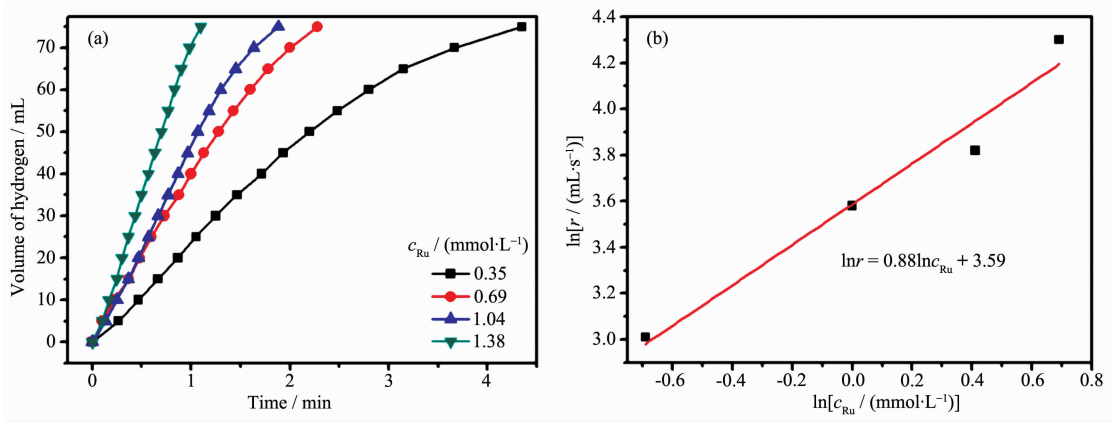

Fig.5 (a) Plots of the volume of hydrogen generation from AB hydrolysis as a function of time at different catalyst concentrations catalyzed by Ru/Ce(OH)CO_3 NCs (c_{AB}=200 mmol·L^{-1}); (b) lnc_{Ru} vs ln$r$ plot

to 1.1 min for complete hydrogen release and the hydrogen generation rate rises gradually. The hydrogen generation rate was determined from the linear portion from 0 to 70 mL of each plot. As shown in Fig.5b, the line slope of the plot of hydrogen evolution rate versus catalyst concentration in a log-log scale is 0.88, indicating that the hydrolysis of AB catalyzed by Ru/Ce(OH)CO_3 NCs are first order with respect to the catalyst concentration. Therefore, the hydrogen generation rate (r) increases by increasing catalyst concentration as expected (*i.e.*, ln$r$=lnc_{Ru}+3.59). Another set of experiments were carried out to study the effect of substrate concentration on the hydrogen generation rate. Fig.S12a shows the plot of the evolution of AB versus time for the hydrolysis of different AB concentrations using a constant Ru/Ce(OH)CO_3 NCs concentration at 1.38 mmol·L^{-1} as the catalyst at (25±0.5) ℃. As shown in Fig.S12b, the line slope of the plot of hydrogen evolution rate versus initial concentration of AB, both in a log-log scale is 0.005, indicating a nearly zero-order regarding the AB concentration. The hydrogen generation rate keeps constant (ln$r$=4.2) for different AB concentrations from the catalytic hydrolysis of AB.

In the final set of kinetic studies, the catalytic hydrolysis of AB was carried out at various temperatures in the range of 20~35 ℃. Obviously, as the reaction temperature increasing from 20 to 35 ℃, the hydrogen generation rates increase quickly (Fig.6a). The values of rate constant k at different temperatures are calculated from the slope of the linear part of each plot from Fig.6a. The Arrhenius plot of ln$k$ vs 1/T for the catalyst is plotted in Fig.6b, from which the apparent activation energy is determined to be

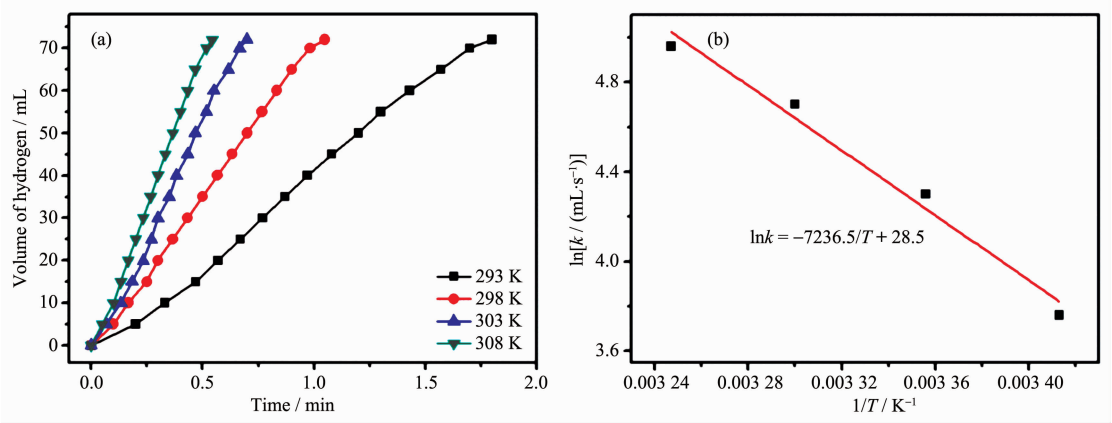

Fig.6 (a) Plot of the volume of hydrogen generation from AB hydrolysis as a function of time at different temperatures catalyzed by Ru/Ce(OH)CO_3 NCs (n_{Ru}/n_{AB}=0.006 9); (b) ln$k$ vs 1/T plot

approximately 60.16 $kJ\cdot mol^{-1}$.

3 Conclusions

In summary, the hydrogen production by hydrolysis of AB was studied by using Ru^0 NPs immobilized on $Ce(OH)CO_3$. Ru NPs with average diameter about 4.8 nm were remarkably well-dispersed on the $Ce(OH)CO_3$. The synthesized $Ru/Ce(OH)CO_3$ NCs exhibited a superior catalytic activity for the hydrolytic dehydrogenation of AB under ambient atmosphere at room temperature. The TOF for the hydrolysis of AB in the presence of $Ru/Ce(OH)CO_3$ NCs were measured to be 389.6 $mol_{H_2}\cdot mol_{Ru}^{-1}\cdot min^{-1}$. Moreover, $Ru/Ce(OH)CO_3$ nanocatalyst was reused for at least eleven cycles in complete hydrolysis of AB. This simple synthetic method can be extended to other $Ce(OH)CO_3$-based metallic systems in more applications.

Supporting information is available at http://www.wjhxxb.cn

References:

[1] Zhang K, Han P, Hu Z, et al. *Chem. Soc. Rev.*, **2015**,**44**(3):699-728

[2] Demirci U B, Miele P. *Energy Environ. Sci.*, **2011**,**4**(9):3334-3341

[3] Han M, Zhao Q, Zhu Z, et al. *Nanoscale*, **2015**,**7**(43):18305-18311

[4] Lu Z H, Yao Q, Zhang Z, et al. *J. Nanomater.*, **2014**,**2014**:729029

[5] Chandra M, Xu Q. *J. Power Sources*, **2006**,**156**(2):190-194

[6] Yao Q, Lu Z H, Wang Y, et al. *J. Phys. Chem. C*, **2015**,**119**(25):14167-14174

[7] Yao Q, Lu Z H, Huang W, et al. *J. Mater. Chem. A*, **2016**,**4**(22):8579-8583

[8] Chen Y Z, Xu Q, Yu S H, et al. *Small*, **2015**,**11**(1):71-76

[9] Yan J M, Wang Z L, Wang H L, et al. *J. Mater. Chem.*, **2012**,**22**(22):10990-10993

[10]Lu Z H, Jiang H L, Yadav M, et al. *J. Mater. Chem.*, **2012**,**22**(11):5065-5071

[11]Yan J M, Zhang X B, Akita T, et al. *J. Am. Chem. Soc.*, **2010**,**132**(15):5326-5327

[12]Aijaz A, Karkamkar A, Choi Y J, et al. *J. Am. Chem. Soc.*, **2012**,**134**(34):13926-13929

[13]Chen W, Ji J, Duan X, et al. *Chem. Commun.*, **2014**,**50**(17):2142-2144

[14]Wang S, Zhang D, Ma Y, et al. *ACS Appl. Mater. Interfaces*, **2014**,**6**(15):12429-12435

[15]Yao Q, Shi W, Feng G, et al. *J. Power Sources*, **2014**,**257**:293-299

[16]Abo-Hamed E K, Pennycook T, Vaynzof Y, et al. *Small*, **2014**,**10**(15):3145-3152

[17]Chen G, Desinan S, Nechache R, et al. *Chem. Commun.*, **2011**,**47**(22):6308-6310

[18]Yao Q, Lu Z H, Jia Y, et al. *Int. J. Hydrogen Energy*, **2015**,**40**(5):2207-2215

[19]Zhang Z, Lu Z H, Tan H, et al. *J. Mater. Chem. A*, **2015**,**3**(46):23520-23529

[20]Shen J, Yang L, Hu K, et al. *Int. J. Hydrogen Energy*, **2015**,**40**(2):1062-1070

[21]Akbayrak S, Kaya M, Volkan M, et al. *Appl. Catal. B*, **2014**,**147**:387-393

[22]Li D, Han J, Han L, et al. *J. Environ. Sci.*, **2014**,**26**(7):1497-1504

[23]Chen J, Lu Z H, Wang Y, et al. *Int. J. Hydrogen Energy*, **2015**,**40**(14):4777-4785

[24]Yao Q, Huang M, Lu Z H, et al. *Dalton Trans.*, **2015**,**44**(3):1070-1076

[25]Yang Y, Lu Z H, Hu Y, et al. *RSC Adv.*, **2014**,**4**(27):13749-13752

[26]Kaya M, Zahmakiran M, Özkar S, et al. *ACS Appl. Mater. Interfaces*, **2012**,**4**(8):3866-3873

[27]Yao Q, Lu Z H, Zhang Z, et al. *Sci. Rep.*, **2014**,**4**:7597

[28]Yan J M, Zhang X B, Han S, et al. *Angew. Chem. Int. Ed.*, **2008**,**47**(12):2287-2289

[29]Lu Z H, Li J, Zhu A, et al. *Int. J. Hydrogen Energy*, **2013**,**38**(13):5330-5337

[30]Glüer A, Förster M, Celinski V R, et al. *ACS Catal.*, **2015**,**5**(12):7214-7217

[31]Wang H L, Yan J M, Wang Z L, et al. *Int. J. Hydrogen Energy*, **2012**,**37**(13):10229-10235

[32]Shan X, Du J, Cheng F, et al. *Int. J. Hydrogen Energy*, **2014**,**39**(13):6987-6994

[33]Lu Z H, Li J, Feng G, et al. *Int. J. Hydrogen Energy*, **2014**,**39**(25):13389-13395

[34]Metin O, Mazumder V, Ozkar S, et al. *J. Am. Chem. Soc.*, **2010**,**132**(5):1468-1469

[35]Wang H, Zhao Y, Cheng F, et al. *Catal. Sci. Technol.*, **2016**,**6**(10):3443-3448

[36]Sahiner N, Yasar A O. *Int. J. Hydrogen Energy*, **2014**,**39**(20):10476-10484

[37]YANG Yu-Wen(杨宇雯), FENG Gang(冯刚), LU Zhang-Hui

(卢章辉), et al. *Acta Phys.-Chim. Sin.*(物理化学学报), **2014**, **30**(6),1180-1186

[38]Yu P J, Lee M H, Hsu H M, et al. *RSC Adv.*, **2015**,**5**(18): 13985-13992

[39]Wang X, Liu D, Song S, et al. *Chem. Commun.*, **2012**,**48** (82):10207-10209

[40]Gao K, Zhu Y Y, Tong D Q, et al. *Chin. Chem. Lett.*, **2014**, **25**(2):383-386

[41]ZHANG Ze-Fang(张泽芳), YU Lei(俞磊), LIU Wei-Li(刘卫丽), et al. *Chinese J. Inorg. Chem.*(无机化学学报), **2011**,**27** (4):759-763

[42]Zhu F, Chen G, Sun S, et al. *J. Mater. Chem. A*, **2013**,**1**(2): 288-294

[43]Qao Q, Lu, Z H, Yang K, et al. *Sci. Rep.*, **2015**,**5**:15186

[44]Chen J, Qao Q, Zhu J, et al. *Int. J. Hydrogen Energy*, **2016**, **41**(6):3946-3954

[45]Rachiero G P, Demirci U B, Miele P. *Catal. Today*, **2011**, **170**(1):85-92

[46]Qadir K, Joo S H, Mun B S, et al. *Nano Lett.*, **2012**,**12**(11): 5761-5768

[47]Dai H B, Kang X D, Wang P. *Int. J. Hydrogen Energy*, **2010**,**35**(19):10317-10323

[48]Joo S H, Park J Y, Renzas J R, et al. *Nano Lett.*, **2010**,**10** (7):2709-2713

[49]Can H, Metin Ö. *Appl. Catal. B*, **2012**,**125**:304-310

[50]Chen G, Sun S, Zhao W, et al. *J. Phys. Chem. C*, **2008**,**112** (51):20217-20221

[51]Wang L, Zhang L F, Zhong S L, et al. *Appl. Surf. Sci.*, **2012**, **263**:769-776

[52]Li X, Zeng C, Fan G. *Int. J. Hydrogen Energy*, **2015**,**40**(10): 3883-3891

[53]Liang H, Chen G, Desinan S, et al. *Int. J. Hydrogen Energy*, **2012**,**37**(23):17921-17927

[54]Akbayrak S, Özkar S. *ACS Appl. Mater. Interfaces*, **2012**,**4** (11):6302-6310

[55]Rakap M. *Appl. Catal. A*, **2014**,**478**:15-20

[56]Durap F, Zahmakıran M, Özkar S. *Appl. Catal. A*, **2009**,**369** (1):53-59

[57]Hu Y, Wang Y, Lu Z H, et al. *Appl. Surf. Sci.*, **2015**,**341**: 185-189

[58]Sahiner N, Demir S, Yildiz S. *Colloids Surf. A*, **2014**,**449**: 87-95

[59]Yan J M, Zhang X B, Shioyama H, et al. *J. Power Sources*, **2010**,**195**(4):1091-1094

[60]Peng C Y, Kang L, Cao S, et al. *Angew. Chem. Int. Ed.*, **2015**,**54**(52):15725-15729